

# 3-D visualisation, printing, and volume determination of the tracheal respiratory system in the adult desert locust, *Schistocerca gregaria*

Mark Greco<sup>1,2\*</sup>, Duncan Bell<sup>3,4</sup>, Lewis Woolnough<sup>5</sup>, Stephen Laycock<sup>4</sup>, Nick Corps<sup>6</sup>, David Mortimore<sup>7</sup> & Diana Hudson<sup>8</sup>

<sup>1</sup>Department of Biology and Biochemistry, University of Bath, Bath BA2 7AY, UK, <sup>2</sup>INVERT Group, Department of Electrical and Electronic Engineering, University of Bath, Bath BA2 7AY, UK, <sup>3</sup>East Anglia Radiography Research, Modelling and 3-D Printing Group, School of Science, Technology and Health, University Campus Suffolk, Ipswich IP4 1QJ, UK, <sup>4</sup>School of Computing Sciences, UEA Norwich, Norwich NR4 7TJ, UK, <sup>5</sup>Quekett Microscopical Club, c/o The Natural History Museum, Cromwell Road, London SW7 5BD, UK, <sup>6</sup>Bruker UK, Banner Lane Coventry, Coventry CV4 9GH, UK, <sup>7</sup>Newbourne Solutions, Newbourne, Woodbridge IP12 4NR, UK, and <sup>8</sup>Department of Biology, Wycombe Abbey School, High Wycombe, Bucks HP11 1PE, UK

Accepted: 31 March 2014

**Key words:** micro-CT, trachea, STL file, Orthoptera, Acrididae, X-ray scanning, diagnostic radioentomology

## Abstract

Here, we describe a single micro-CT scan with a spatial resolution of 10  $\mu\text{m}$  of a 10-day-old adult male *Schistocerca gregaria* (Forskål) (Orthoptera: Acrididae) and we compare our tracheal volume ( $V_T$ ) determination with published work on the subject. We also illustrate the feasibility of performing non-invasive ‘virtual dissection’ on insects after performing micro-CT. These post-processing steps can be performed using free downloadable 3-D software. Finally, the values of producing stereo-lithography (STL) files that can be viewed or used to print out 3-D models as teaching aids are discussed.

## Introduction

The intricate tracheal respiratory system that delivers oxygen directly to tissues and cells is a distinctive feature of many arthropods (Chapman, 1998; Lease et al., 2006). In terrestrial arthropods, the tracheal system plays a vital role in delivering oxygen from the atmosphere directly to cells via the haemolymph and in expelling carbon dioxide derived from cellular respiration back into the atmosphere. In 2006, Lease et al. determined that the tracheal volume ( $V_T$ ) of one group of terrestrial arthropods (the insects) should be considered as the total volume of air in the tracheae and air sacs combined. Because the vast majority of insects have a paucity of the oxygen-carrying respiratory proteins haemocyanin and haemoglobin (Chapman, 1998),  $V_T$  greatly determines the amount of oxygen available during insect respiration when the spiracles are closed (Lease et al., 2006). The relationship

between insect  $V_T$  and ontogeny is complex.  $V_T$  varies according to body size, metabolic rate, species type, presence/absence of air sacs, developmental stage, and the individual's reproductive or digestive status (Lease et al., 2006).

Various methods have been used to determine  $V_T$  in insects, including water displacement (Wigglesworth, 1950), use of inert gases (Bridges et al., 1980; Lease et al., 2006), stereology (Schmitz & Perry, 1999; Hartung et al., 2004; Snelling et al., 2011, 2012), and stereology in combination with synchrotron X-ray imaging (Kaiser et al., 2007; Greenlee et al., 2009; Socha et al., 2010; Kirton et al., 2012). All have potential advantages and disadvantages. Insect imaging is being revolutionised by the use of X-ray Synchrotron imaging (Kaiser et al., 2007; Greenlee et al., 2009; Socha et al., 2010; Greco et al., 2011b, 2012; Kirton et al., 2012); however, adequate long-term access to synchrotron facilities is a limiting factor for entomologists who require non-invasive approaches to their research.

Nevertheless, visualising the anatomy of an entire insect tracheal system including the use of modern stereomicroscopes remains notoriously difficult (Vinal, 1919;

\*Correspondence: Mark Greco, Department of Biology and Biochemistry, University of Bath, Bath BA2 7AY, UK.  
E-mail: m.k.greco@bath.ac.uk

Snodgrass, 1935; Albrecht, 1953, 1956; Miller, 1960a,b,c; Clarke & Richards, 1976). In 1919, Vinal eloquently illustrated the respiratory system of the Carolina locust, *Dissosteira carolina* (L.) and summarised and referenced much of the earlier work on locust tracheal systems. The article included Malpighi's discovery of the respiratory system of the silk worm in 1669 and the beautifully illustrated work of Swammerdam on honey bee anatomy published in 1673. Vinal (1919) also details the work of others including Lyonet (1762) on the goat moth *Cossus cossus* L., Strauss-Durckheim (1828) on the cockchafer *Melolontha vulgaris* (L.) and Denny's studies of the cockroach, and finally the studies of Alt (1912) on the great diving beetle, *Dytiscus marginalis* L.

Much of the research on insect respiration from the 1970s onwards (Richards & Davies, 1977; Chapman, 1998; Klowden, 2007; Nation, 2008) continues to refer back to the early research of Swammerdam (1673), Vinal (1919), and Snodgrass (1935). Research on respiratory physiology on the mechanisms of insect ventilation and flight frequently refers to research from Hamilton (1937), Weis-Fogh (1952, 1956a,b,c, 1964a,b,c, 1967), and Miller (1960a,b,c), and to the detailed light and electron microscopic studies of tracheal and air sac anatomy (Maina, 1989; Hartung et al., 2004). This common practise of referring to historical studies reflects the continuing difficulties with dissecting extremely small (10–20 µm) and delicate tracheae and air sacs (Vinal, 1919). Such problems include (1) obstruction or alteration of exact anatomical and spatial relationships due to air sacs expanding and shifting as soon as the insect is opened, particularly with the insect under water or a preservative liquid, and (2) air sacs/tracheae are often situated between muscle layers in the thorax or fat bodies and ovaries in the abdomen and it is almost impossible to dissect these out without severing much of the connecting tracheal network. Subsequently, alternative methods to demonstrate tracheal anatomy such as direct injection of various dyes into the tracheal system (Wigglesworth, 1950) and corrosion casting plus scanning electron microscopy (Meyer, 1989) have been attempted.

X-ray computerised tomography methods are being used increasingly by entomologists (Hornschemeyer et al., 2002; Honnickea et al., 2005; Greco et al., 2005, 2006, 2008, 2009, 2011a, 2012) to visualise and study nest architecture and insect morphology, physiology, and behaviour. In 2008, we hypothesised that micro-CT would be a suitable method for visualising the insect tracheal system (Al-Harbi, 2008) and we attempted to quantify changes in abdominal air sac size that occur during insect digestion. The terrestrial arthropod we chose was the desert locust, *Schistocerca gregaria* (Forskål) (Orthoptera: Acrididae), because its anatomy and that of several similar acridids

have been well documented (Vinal, 1919; Snodgrass, 1935; Misra, 1945, 1946, 1947).

Our early results supported the hypothesis of Al-Harbi (2008, 2008). We have subsequently developed more sophisticated software to analyse insect micro-CT data (Bell et al., 2012; Greco et al., 2012) and we have augmented our methods by including 3-D printed models which we generate from macro-CT (Hulse et al., 2012) and micro-CT data (Laycock et al., 2012).

Here, we describe the methods used and the results obtained from a single micro-CT scan of a 10-day-old adult male *S. gregaria* and we compare our results for  $V_T$  determination with published work on the subject. We also illustrate the feasibility of performing non-invasive 'virtual dissection' on insects after performing micro-CT. These post-processing steps can be performed using free downloadable 3-D software. Finally the value of producing STL (stereo-lithography) files that can be viewed or used to print out 3-D models as a teaching aid is discussed.

## Materials and methods

### The insect

At 10 days post-moult of the adult stage, a male *S. gregaria* was randomly selected from a stock of caged experimental locusts that were kept at 26 °C, 40% r.h., and L12:D12 photoperiod. The cages were equipped with a 60-W light bulb. Locusts were fed on wheat bran and fresh wheat shoots and provided with distilled water periodically treated with 5% antiprotozoal solution (wt/vol; 4.26% sodium sulphamethazine, 3.65% sodium sulphathiazole, 3.13% sodium sulphamerazine) to prevent infection from the sporozoan parasite *Malamoeba locustae* (King & Taylor). To obtain sharp images during the scan, it is very important that the temperature of the sample reaches equilibrium with room temperature before the scan starts. The high spatial resolution for this experiment, 10.469 µm, would cause even minor temperature-induced expansion or contraction to blur the reconstructed cross-sectional images. Therefore, prior to scanning, the specimen was left at room temperature for 24 h in a sealed acrylic tube. To avoid shrinkage of structures during scans due to dehydration, we mounted the locust in a sealed tube containing some free saline during the scan. No shrinkage related artefacts were visible in the resulting cross-sectional images.

### Micro-CT scanning

The methods used are described in greater detail by Tarplee & Corps (2008). The 10-day-old male was killed by placing in the deep freeze at –20 °C and micro-CT scanned approximately 2 days later. The scanned insect was suspended vertically in a 30-mm acrylic tube that was

mounted tightly on the micro-CT's inclination stage. This stage was used to ensure that the rotation axis was at 90° to the x-ray source. Exposure factors were: kVp = 50 and  $\mu\text{A} = 198$ . The data were isotropic 16 bit 2000 × 2000 with 1 048 rows. Pixel size was 10.469  $\mu\text{m}$ .

#### Image reconstruction and viewing

Skyscan NRecon software version 1.5.1.4 was used to reconstruct the projection data (Tarplee & Corps, 2008). Having obtained the projection data in the form of an image stack of 2-D TIFF (tagged image file format) files the data was viewed as a 3-D model using disect software, DISECT Systems ([www.disectsystems.com](http://www.disectsystems.com); Greco et al., 2012).

#### Masking and segmenting

The TIFF image stacks were loaded into the masking and segmenting software 'Tomomask' at full resolution ([www.tomomask.com](http://www.tomomask.com)). The application of the masking features within the software enabled 'virtual' removal of the acrylic tube surrounding the locust before performing various 'virtual' dissections to remove the legs and wings as follows.

The TIFF image stacks were loaded into TomoMask at full resolution. The acrylic tube surrounding the locust was 'removed' from the images by painting with the background grey tone, i.e., black. Next, in a similar manner a series of virtual dissections were performed to remove the legs and wings. From these masking operations, new image stacks were created consisting of the locust body only, front leg, middle leg, rear leg, and wings. These image stacks were then reloaded into TomoMask one-by-one and the tracheae/air sacs were segmented by replacing the black connected regions of the air sacs with white. This was done automatically using the 3-D connected threshold function of TomoMask. Care was taken to ensure that where the tracheae exited the body of the locust, a barrier mask was applied to prevent the air external to the locust from being included in the 3-D connected region. To calculate the volume of the tracheae/air sacs, the voxel volume was multiplied by the number of segmented 'white' pixels. As the entire Micro-CT scan is composed of 3-D voxels, we used Tomomask's voxel statistics feature and tallied the voxel values obtained from the dissected legs, wings, head, thorax, and abdomen to calculate the  $V_T$ .

#### Production of 3-D printed models

When we were satisfied with the segmenting process of the tracheal system with the legs, wings, head, thorax, and abdomen, the files were saved and converted to STL files by using the marching cubes algorithm within TomoMask. These STL files are available for download

at [www.fishersideas/Papers/LocustTrachea](http://www.fishersideas/Papers/LocustTrachea). We then viewed in 3-D by using the freely available software (Meshlab: <http://meshlab.sourceforge.net/>) and printed out as 3-D model using a 3-D printer (Z-Corps 450: <http://www.zcorp.com/en/home.aspx>).

#### Validating volume accuracy

To confirm the accuracy of our volume estimations, we scanned six insulin syringes (Terumo, Egham, UK) using the same parameters as for the locust scan. Importantly the parameters such as scanning at 9.01 microns are the same as those used for the locust scan. The syringes are designed so that 300  $\mu\text{l}$  is equivalent to 30 units of the U-100 insulin. The external and internal diameters of the syringe are 5 and 3 mm, respectively. The length of the scale from 0 to 30 units is 42 mm. So each 5-unit mark is 7 mm long. There are 10 marks (five large and five small) between each 5-unit mark. The total internal volume of a syringe is 296.856  $\mu\text{l}$  and we moved the plungers to six different positions for the scan. This gave us six volumes to estimate. We used the same syringe volume estimation method as for the locust. We then plotted expected volumes vs. estimated volumes as a linear regression with best line of fit.

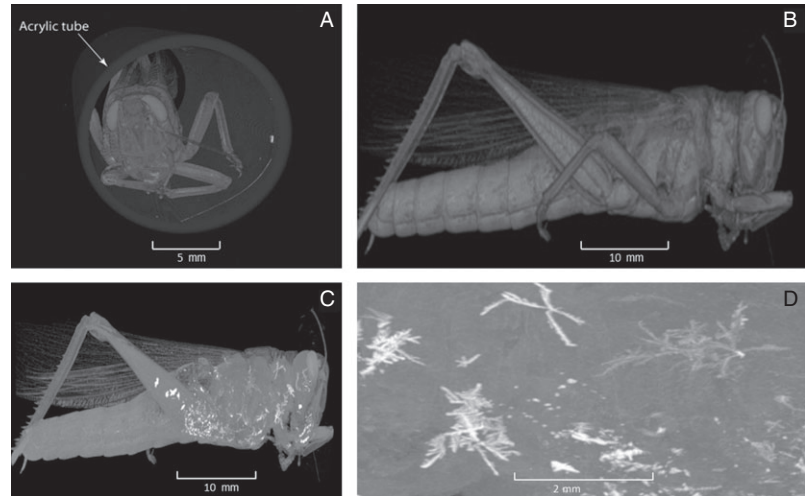
We also compared the linear measurements (using digital callipers) obtained from the diameter of the syringe with that obtained from the micro-CT scan. Again these correlate well.

## Results

### Imaging

Initially, the 3-D views of the insect were obscured by the acrylic tube (Figure 1A). However, masking and segmentation of the tube (Figure 1B) enabled full visualisation of the locust externally including cuticular details. High-attenuation structures (HAS) within the muscular tissues of the head, thorax, and proximal metathoracic femora and a notable absence of HAS in the abdomen were observed (Figure 1C). At greater magnification (Figure 1D) details of the ramiform nature of some of the intra-thoracic HAS can be seen. High, medium, and low attenuation structures were observed, varying from very dense structures (grey scale between +230 and +4 000), such as the zinc-containing mandibles (Hillerton & Vincent, 1982; Al-Harbi, 2008), to very low-density air-filled structures (grey scale between -4 000 and 0), such as air sacs and larger tracheae (Figure 2A). The grey-scale values for soft-tissue structures such as muscle and the brain ranged from +30 +279 to +35 +300 and were visualised as various shades of grey. Figure 2B shows the tergo-ventral muscles, dorsal longitudinal muscles, air sacs, and

**Figure 1** Four 3-D views of the desert locust (*Schistocera gregaria*). (A) Obscured by the acrylic tube. (B) After masking and segmenting the tube showing cuticular details. (C) Evidence of the high-attenuation structures (HAS) as white ramiform structures within the muscular tissues of the head, thorax, and proximal metathoracic femora, but not in the abdomen. (D) Greater magnification of the HAS to show detail of the ramiform patterns.



tracheae clearly in a 3-D transverse section through the prothorax at the level of the first thoracic spiracle. The hollow 'pegs' arising from the pleural surface of the prothorax which keep the pronotum clear of the spiracular orifice are also clearly seen. Figure 2C demonstrates the ability to produce oblique, 3-D cut away virtual 'dissections' at an infinite number of angles (Greco et al., 2005).

This enabled a longitudinal oblique view with removal of the legs to demonstrate the orifices of the first and second thoracic and first abdominal spiracles. Figure 2D accurately demonstrates the tympanum, which is difficult to visualise without physical dissection, including the tympanic membrane, camera tympanum, and the thoracic air sacs positioned between them.

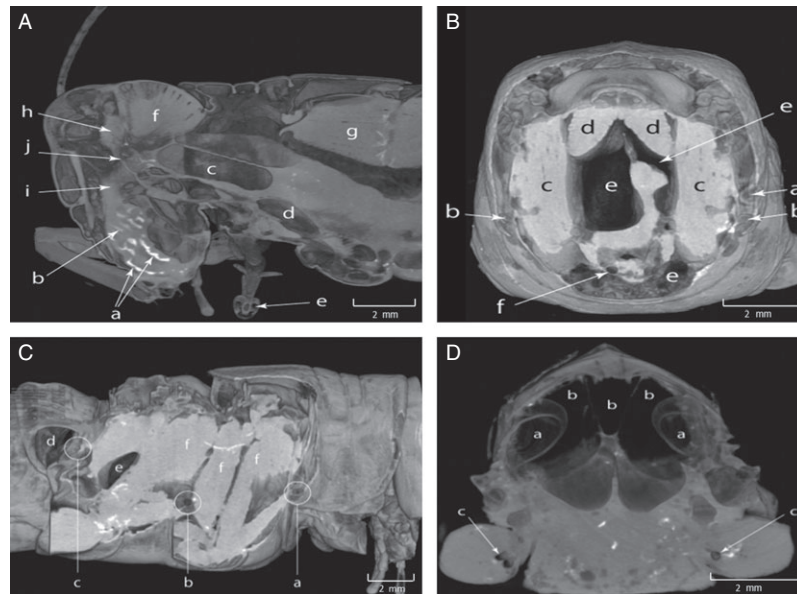


**Figure 2** Four 3-D views of the head and thorax. (A) Sagittal view of the mandibular incisors (a), mandibular molars (b), air in the oesophagus (c), air sacs (d), tracheae (e), mandibular adductor muscles (f), prothoracic dorsal longitudinal muscles (g), brain (h), pharynx (i), and the circumoesophageal commissures (j). (B) Transverse view through the prothorax at the level of the first thoracic spiracle showing the hollow 'pegs' (a) arising from the pleural surface of the prothorax (b), tergo-ventral muscles (c), dorsal longitudinal muscles (d), air sacs (e), and tracheae (f). (C) Oblique longitudinal view with legs and wings segmented showing the orifices of the first (a) and second (b) thoracic and first abdominal (c) spiracles, camera tympanum (d), thoracic air sacs (e), and tergo-ventral muscles and interposed air sacs with one of the high-attenuation structures traversing them (f). (D) Transverse view at the level of the first abdominal section showing fine detail of the camera tympanum (a), abdominal air sacs between the tympana (b), and tracheae in the proximal metathoracic femora (c).

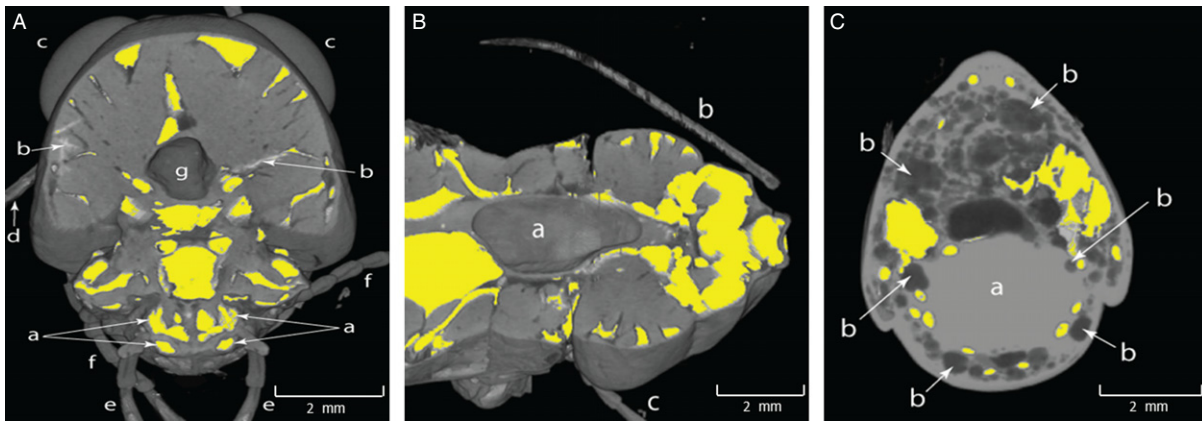


**Figure 3** Three views of the head and thorax. (A) 3-D transverse view of small air sacs within the labium (a), high-attenuation structures (HAS) (b), compound eyes (c), left antenna (d), labial palps (e), maxillary palps (f), and air in the gut (g). (B) 3-D horizontal view of head, cervix, and anterior prothorax showing air in the crop (a), left antenna (b), and right maxillary palp (c). The tracheae and air sacs were also well visualised. (C) 2-D transverse view through the abdomen. (C) 2-D transverse section through the abdomen showing the tracheal system (yellow) with the visceral tracheal plexus surrounding the gut (a) and the fat bodies (b) dispersed throughout the abdomen.

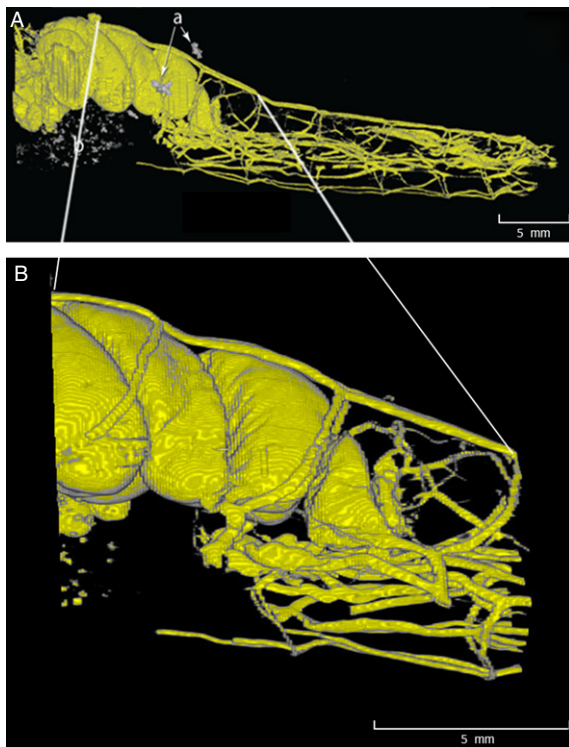


**Figure 4** Two 3-D views of the segmented tracheal system. (A) 3-D view of the segmented thoracic and abdominal tracheae with the high-attenuation structures in the proximal metathoracic femora (a) and meta- and mesothoracic muscles (b). (B) Enlarged 3-D section of the distal thoracic and proximal abdominal tracheal system to show fine structural details.

Figure 3 shows a 3-D view of the locust's head and thorax, that has been virtually dissected transversely at the level of the cervix (Figure 3A), virtually dissected horizontally at the level of the posterior cibarium/anterior oesophagus (3B), and virtually dissected transversely at the mid thoracic level (3C). The ring of perivisceral tracheae surrounding the gut is particularly well shown as are those in the proximal metathoracic legs. We were able to demonstrate the entire 3-D segmented tracheal system with some of the HAS (Figure 4A) and an enlarged 3-D view of the thoracic section to show finer detail of tracheoles (4B). Details of legs, HAS, and tracheae including the left prothoracic leg tracheal system and prothoracic HAS (Figure 5A), the mesothoracic HAS and tracheal system of the corresponding right leg (5B), and the metathoracic HAS and the tibial spur tracheae of the left metathoracic leg (5C) were shown. The left forewing segmented to reveal the left tympanum and first abdominal spiracle (Figure 6). The estimated combined tracheal volume of the legs, head, thorax, and abdomen was 253  $\mu\text{l}$ .

#### The 3-D printed model

Examples of the interactive STL files that were reconstructed (Figure 7) can be downloaded at [www.fishersideas.co.uk/Papers/LocustTrachea/LocustTrachea.html](http://www.fishersideas.co.uk/Papers/LocustTrachea/LocustTrachea.html). An STL file of one and a half abdominal segments of the locust with a 'U' shaped structural support added to the image prior to printing was reconstructed (Figure 8A) and a physical powder 3-D model produced using Zp150 powder (8B) in a 3-D printer (Z-Corps 450: <http://www.zcorp.com/en/home.aspx>).

### Syringe measurements

**Volume.** As seen from Figure 9, the simple linear regression equation is: Micro-CT estimated volume ( $\mu\text{l}$ ) =  $1.034 \times$  insulin syringe volume ( $\mu\text{l}$ ) - 1.171 [slope SE = 0.034, 95% confidence interval (CI) for population value of slope = 0.939–1.129]. Correlation coefficient ( $r$ ) = 0.998 [95% CI for  $r$  (Fisher's Z transformed) = 0.979–1.0], which is significantly different from 0 ( $t = 30.181$ , d.f. = 4,  $P < 0.0001$ ).

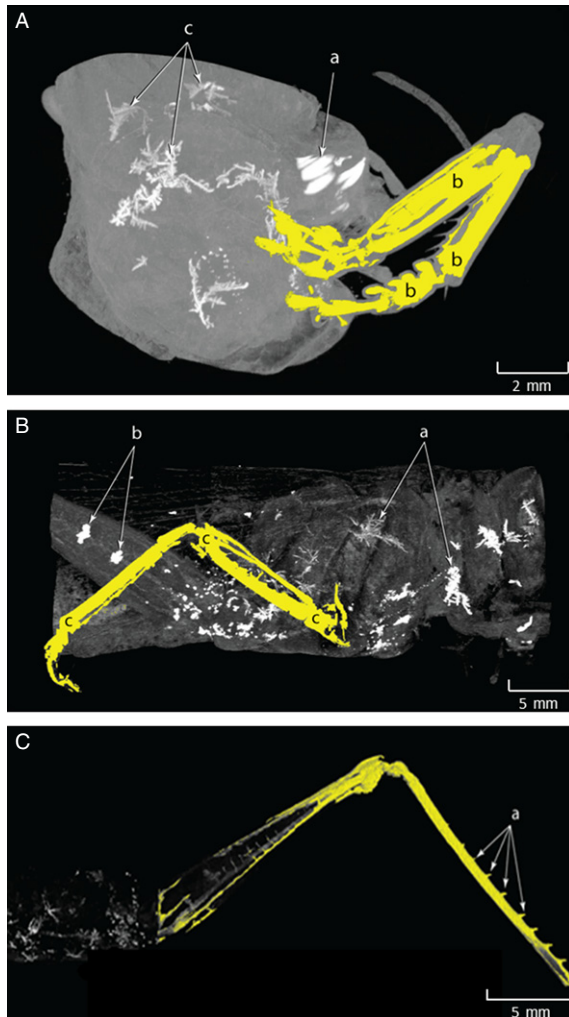


**Figure 5** Three maximum intensity projection (MIP) volume rendered images of the thorax including details of legs, high-attenuation structures (HAS) and tracheae. (A) Mandibular teeth (a), left prothoracic leg tracheal system (b), and prothoracic HAS (c). (B) Mesothoracic HAS (a), metathoracic leg HAS (b), and tracheal system of the corresponding right leg (c). (C) Metathoracic HAS and tibial spur tracheae of the left metathoracic leg (a).

**Linear dimensions.** As seen from Figure 10, the simple linear regression equation is: Linear measurements (mm) using micro-CT =  $0.996 \times$  linear measurements (mm) using digital callipers + 0.055 (slope SE = 0.0106, 95% CI for population value of slope = 0.969–1.023). Correlation coefficient ( $r$ ) > 0.999 [95% CI for  $r$  (Fisher's Z transformed) = 0.998–1.0], which is significantly different from 0 ( $t = 94.018$ , d.f. = 5,  $P < 0.0001$ ).

### Discussion

To our knowledge, our methods show the first account of non-invasive measurement of an insect tracheal volume and detailed, physical 3-D models of the anatomy of an individual insect's respiratory system. All previous attempts have been produced with prior knowledge gained from physical dissections or other destructive methods. Thus, by definition, those approaches are estimations and prone to large errors. Our results show that it is straightforward to demonstrate tracheal anatomy in insects using a micro-CT and appropriate software. The ready conversion of the image stack data to an STL format allows the complex 3-D anatomy of the respiratory system of the locust to be clearly seen.

The tracheal volume we obtained of  $253 \mu\text{l}$  is in accordance with volume estimates based on published methods,

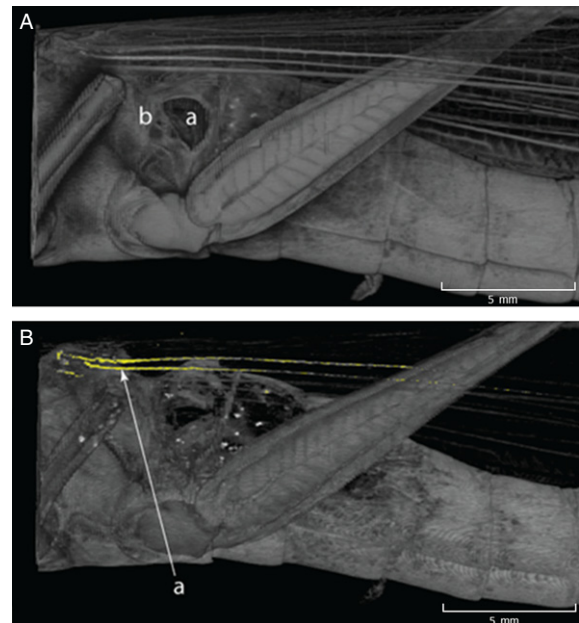


**Figure 6** Two 3-D views of the metathorax and anterior abdomen. (A) Left forewing segmented to reveal the left tympanum (a) and first abdominal spiracle (b). (B) For greater detail, the fine tracheae in the hind wing has been masked (a).



**Figure 7** Stereo-lithography file of the segmented tracheal system of the locust's abdominal tracheal system.

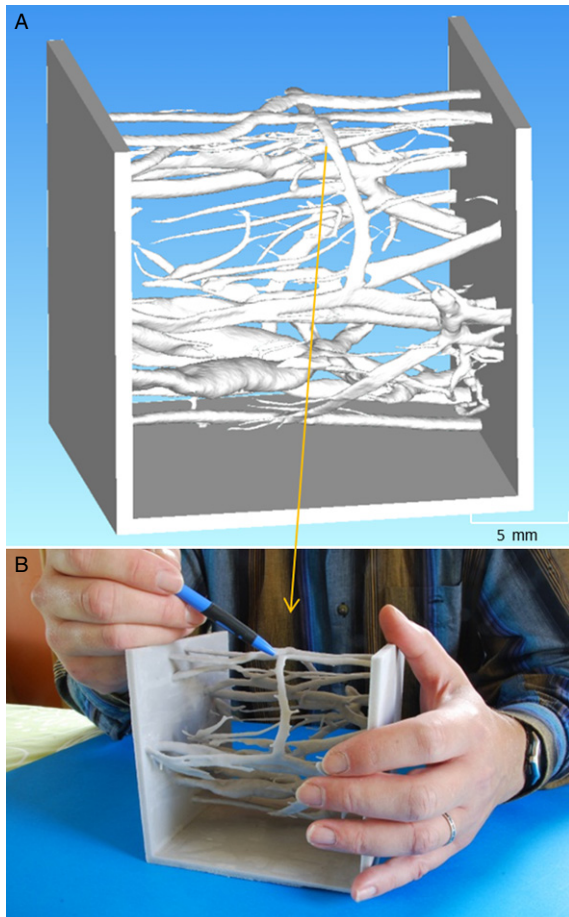


**Figure 8** Stereo-lithography image of a section of the segmented tracheal system of the locust's abdominal tracheae (A) and a photograph of the physical 3-D model to be used as a teaching aid. The instructor is pointing out an abdominal collateral bridging trachea (B).

such as water displacement (Wigglesworth, 1950), inert gases (Bridges et al., 1980; Lease et al., 2006), stereology (Schmitz & Perry, 1999; Hartung et al., 2004), and stereology in combination with synchrotron X-ray imaging (Kaiser et al., 2007; Greenlee et al., 2009; Socha et al., 2010; Kirton et al., 2012).

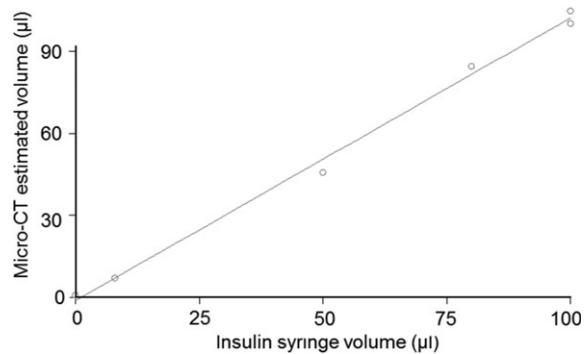


**Figure 9** Simple linear regression of estimated vs. expected volume of six syringes with plungers at different positions.

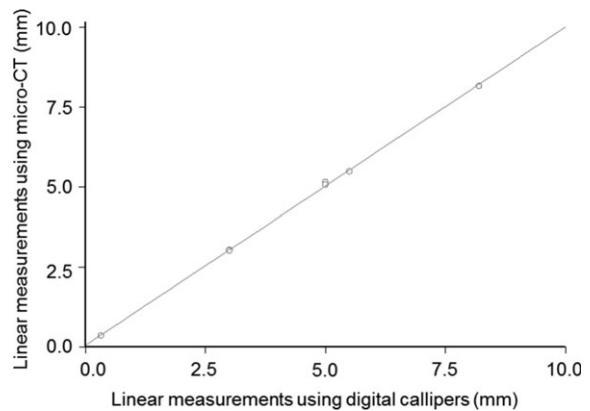


**Figure 10** Simple linear regression of estimated vs. expected linear distances of six syringes with plungers at different positions.

When we used the Tomomask software to segment out the air-filled tracheal system, there was no filling of other air-filled spaces within the locust such as air in the crop or the extra oral space. Thus, there were no problems when segmenting out the abdominal tracheal system. However, we did experience 'leaks' from inside out at a few predictable places due to the 'partial volume' effect (Tarplee &

Corps, 2008) where the membranous non-sclerotized exoskeleton of the insect was extremely thin, such as the tympanum and the membranous periarticular regions of several of the smaller joints of the legs. This problem was easily solved by using the 'paint' function within Tomomask set at an attenuation of 8 000 to 'patch over' any such potential defects, thus rendering the insect 'leak-proof'.

On theoretical grounds, with an isotropic micro-CT scan taken (as in our study) at a voxel size of approximately 10  $\mu\text{m}$ , one would predict that structures such as tracheae should be reliably detectable down to a size of about 10  $\mu\text{m}$  bearing in mind that the X-ray attenuation of the air in this structure is considerably less than that of the surrounding soft tissue (Tarplee & Corps, 2008). When 3-D voxels are located between regions of different X-ray attenuation they inherently contain partial volume errors. As the voxel size for this study was 10  $\mu\text{m}$ , our method of total respiratory system volume determination would underestimate the value because the voxels were bigger than some of the tracheoles and therefore would be located between different x-ray attenuation regions (e.g., air/muscle) and, as a consequence, would be subjected to partial volume errors. These errors would cause an underestimation of the total respiratory system volume.

However, if one is using our total respiratory system volume determination technique for either 'before and after' type studies in the same live anaesthetised insect (Al-Harbi, 2008) or killed groups of insects (e.g., fed vs. unfed), then the theoretical underestimation of total respiratory system volume will be the same in both groups. We were not able to quantify tracheolar volumes that were smaller than 10  $\mu\text{m}$  in diameter and we estimate that this volume might be as large as 10% of total tracheal volume in adult *Schistocerca* (Snelling et al., 2011, 2012). Therefore our methods are, at the moment, limited. To partially overcome these pixel/voxel size limitations, we intend to conduct further studies on locusts using micro-CT and nano-CT scanners with smaller voxel sizes and thus greater resolution.

The results from this study compare with synchrotron dual phase micro-CT (Kirton et al., 2012); however, we used a cheaper and readily available high resolution bench-top micro-CT scanner. A limiting factor for synchrotron imaging is that, in the entire UK there is currently only one synchrotron scanner and so UK-based research workers such as ourselves might typically have to wait several months for an opportunity to use it.

Shaha et al. (2013) described a similar method to our approach and used seven samples to overcome variances in tracheal volumes. However, to validate the accuracy of

our methods, we scanned six insulin syringes of known volumes. It is worth mentioning that insulin syringes can vary in actual volumes (Ltif & Schwenk, 1999). Thus, we suggest that our methods provide more accurate and reproducible results.

Most researchers using micro-CT for radioentomological studies do not have access (as of course do medically qualified radiologists) to appropriate user-friendly relatively inexpensive viewing, masking, and segmenting software. We have shown that by using Tomomask's 2-D powerful editing features in combination with 'disect's' 3-D viewing and conferencing capabilities it is possible to perform and share the results of virtual and non-destructive 'dissection' of insects. Once one is satisfied with the result(s), these files can be stored for future viewing or converted to STL format and used either again for viewing or alternatively the production of physical 3-D models for teaching purposes.

The nature of the high-attenuation structures (HAS) are at this stage unclear, but they may include dried dead cells accumulated in sections of the tracheae, calcium deposits/scarring after localised infections, aggregations of the locust tracheal mite (*Locustacarus trachealis* Ewing, *Locustacarus buchneri* Macfarlane) or some other species, infected glandular tissue, or accumulated debris from external airborne impurities. We are also considering the hypothesis that these may be effete tracheal structures as described by Miller (1960c). Further micro-CT scans of locusts at 5  $\mu\text{m}$  resolution in conjunction with histological sectioning are currently in progress.

## Acknowledgements

The authors thank Professor Keith Charnley for his assistance with initial micro-CT scanning.

## References

- Albrecht FO (1953) *The Anatomy of the Migratory Locust*. Athlone Press, London, UK.
- Albrecht FO (1956) *The Anatomy of the Red Locust (Nomadacris septemfasciata Serville)*. Anti-Locust Research Centre, London, UK.
- Al-Harbi J (2008) *Use of Micro-CT to Investigate the Configuration of the Tracheal System in the Desert Locust, Schistocerca gregaria*. MPhil Thesis, Department of Biology and Biochemistry, University of Bath, Bath, UK.
- Bell GD, Woolnough L, Mortimore M, Corps N, Hudson DM & Greco MK (2012) A preliminary report on the use of bench-top x-ray micro-computerised tomography to study the malpighian tubules of the overwintering seven spotted ladybird *Coccinella septempunctata* L. (Coleoptera: Coccinellidae). *Psyche* 348348: 1–6.

- Bridges CR, Kestler P & Scheid P (1980) Tracheal volume in the pupa of the saturniid moth *Hyalophora cecropia* determined with inert gases. *Respiratory Physiology* 40: 281–291.
- Chapman RF (1998) *The Insects: Structure and Function*, 4th edn. Cambridge University Press, Cambridge, UK.
- Clarke WM & Richards MM (1976) *The Locust as a Typical Insect*. John Murray, London, UK.
- Greco MK, Spooner-Hart R & Holford P (2005) A new technique for monitoring *Trigona carbonaria* nest content, brood and activity using X-ray computerised tomography. *Journal of Apicultural Research* 44: 97–100.
- Greco MK, Bell M, Spooner-Hart R & Holford P (2006) X-ray computerised tomography as a new method for monitoring *Amegilla holmesi* nest structures, nesting behaviour, and adult female activity. *Entomologia Experimentalis et Applicata* 120: 71–76.
- Greco MK, Jones A, Spooner-Hart R & Holford P (2008) X-ray computerised microtomography (microCT): a new technique for assessing external and internal morphology of bees. *Journal of Apicultural Research and Bee World* 47: 286–291.
- Greco MK, Hoffmann D, Dollin A, Duncan M, Spooner-Hart R & Neumann P (2009) The alternative Pharaoh approach: stingless bees encapsulate beetle parasites alive. *Naturwissenschaften* 97: 319–323.
- Greco MK, Spooner-Hart RN, Beattie GAC, Barchia I & Holford P (2011a) Australian stingless bees improve greenhouse *Capsicum* production. *Journal of Apicultural Research* 50: 102–115.
- Greco MK, Welz PM, Siegrist M, Ferguson J, Gallman P et al. (2011b) Describing an ancient bee trapped in amber using diagnostic radioentomology. *Insectes Sociaux* 58: 487–494.
- Greco MK, Tong J, Soleimani M, Bell GD & Schafer MO (2012) Imaging live bee brains using minimally-invasive diagnostic radioentomology. *Journal of Insect Science* 12: 1–7.
- Greenlee KJ, Henry JR, Kirton SD, Westneat MW, Fezzaa K et al. (2009) Synchrotron imaging of the grasshopper tracheal system and physiological components of tracheal hypermetry. *American Journal of Physiology* 297: 1343–1350.
- Hamilton AG (1937) The mechanism of respiration of locusts and its bearing on the problem of inhalation of poison dusts. *Bulletin of Entomological Research* 28: 53–68.
- Hartung DK, Kirton SD & Harrison JF (2004) Ontogeny of tracheal system structure: a light and electron-microscopy study of the metathoracic femur in the American locust *Schistocerca americana*. *Journal of Morphology* 262: 800–812.
- Hillerton JE & Vincent JFV (1982) The specific location of zinc in insect mandibles. *Journal of Experimental Biology* 101: 333–336.
- Hornschemeyer T, Buetel RG & Pasop F (2002) Head structures of *Priacma serrata* Leconte (Coleoptera, Archostemata) inferred from x-ray tomography. *Journal of Morphology* 252: 298–314.
- Hulse M, Tam M, Isherwood S, Scrase C, Laycock ST et al. (2012) Production of 3-D printer-generated radiotherapy treatment shells using DICOM CT, MRI or 3-D surface laser scan – Acquired STL files: Preclinical feasibility studies. Abstract to be shown at the NCRI National Meeting, Liverpool, 3–5th November 2012.
- Kaiser A, Klok JC, Socha JJ, Lee W-K, Quinlan MC & Harrison JF (2007) Increase in tracheal investment with beetle size supports hypothesis of oxygen limitation on insect gigantism. *Proceedings of the National Academy of Sciences of the USA* 104: 13198–13203.
- Kirton SD, Hennessey LE, Duffy B, Bennett MM, Lee W-K & Greenlee GJ (2012) Intermolt development reduces oxygen delivery capacity and jumping performance in the American locust (*Schistocerca americana*). *Journal of Comparative Physiology B* 182: 217–230.
- Klowden MJ (2007) *Physiological Systems in Insects*, 2nd edn. Elsevier, Amsterdam, The Netherlands.
- Laycock SD, Bell GD, Mortimore DB, Greco MK, Corps N & Finkle I (2012) Combining X-ray Micro-CT technology for the digital preservation and study of a 19th century Cantonese chess piece with intricate internal structure. *Journal on Computing and Cultural Heritage* 5: 13.
- Lease HM, Wolf BO & Harrison JF (2006) Intraspecific variation in the tracheal volume in the American locust, *Schistocerca americana*, measured by a new inert gas method. *Journal of Experimental Biology* 209: 3476–3483.
- Ltief AN & Schwenk WF (1999) Accuracy of pen injectors versus insulin syringes in children with type 1 diabetes. *Diabetes Care* 22: 1.
- Maina JN (1989) Scanning and transmission electron microscopic study of the tracheal air sac system in a grasshopper *Chrotogonus senegalensis* (Kraus) – Orthoptera: Acridae: Pyromorphinae. *Anatomical Record* 223: 393–405.
- Meyer EP (1989) Corrosion casts as a method for investigation of the insect tracheal system. *Cell and Tissue Research* 256: 1–6.
- Miller PL (1960a) Respiration in the desert locust 1. The control of ventilation. *Journal of Experimental Biology* 37: 224–236.
- Miller PL (1960b) Respiration in the desert locust II. The control the spiracles. *Journal of Experimental Biology* 37: 237–263.
- Miller PL (1960c) Respiration in the desert locust III. Ventilation and the spiracles during flight. *Journal of Experimental Biology* 37: 264–278.
- Misra DM (1945) Studies on the somatic musculature of the desert locust, *Schistocerca gregaria* (Forskål), Part I. The head. *Indian Journal of Entomology* 7: 103–138.
- Misra DM (1946) Studies on the somatic musculature of the desert locust, *Schistocerca gregaria* (Forskål), Part 2. The neck and prothorax. *Indian Journal of Entomology* 8: 1–29.
- Misra DM (1947) Studies on the somatic musculature of the desert locust, *Schistocerca gregaria* (Forskål), Part 3. The pterothorax. *Indian Journal of Entomology* 9: 19–72.
- Nation JL (2008) *Insect Physiology and Biochemistry*, 2nd edn. CRC Press, Boca Raton, FL, USA.
- Schmitz A & Perry SF (1999) Stereological determination of tracheal volume and diffusing capacity of the tracheal walls in the stick insect *Carausius morosus* (Phasmatodea, Lonchodidae). *Physiological and Biochemical Zoology* 72: 205–218.

- Shaha RK, Vogt JR, Han C-S & Dillon ME (2013) A micro-CT approach for determination of insect respiratory volume. *Arthropod Structure & Development* 42: 437–442.
- Snelling EP, Seymour RS, Runciman S, Matthews PGD & White CR (2011) Symmorphosis and the insect respiratory system: allometric variation. *Journal of Experimental Biology* 214: 3225–3237.
- Snelling EP, Seymour RS, Runciman S, Matthews PGD & White CR (2012) Symmorphosis and the insect respiratory system: a comparison between flight and hopping muscle. *Journal of Experimental Biology* 215: 3324–3333.
- Snodgrass RE (1935) *Principles of Insect Morphology*. McGraw-Hill, New York, NY, USA.
- Socha JJ, Forster TD & Greenlee KJ (2010) Issues of convection in insect respiration: insights from synchrotron X-ray imaging and beyond. *Respiratory Physiology and Neurobiology* 173S: S65–S73.
- Tam M, Bell GD, Williams S & Heylings D (2007) Making cross-sectional anatomy an accessible adjunct for anatomy education. *Clinical Anatomy* 20: 465–472.
- Tarplee M & Corps N (2008) Skyscan 1072 Desktop X-Ray Microtomograph – Sample Scanning, Reconstruction, Analysis and Visualisation (2-D & 3-D) Protocols. Guidelines, Notes, Selected References and FAQ. Available at: <http://www.geog.qmul.ac.uk/docs/staff/4952.pdf> (accessed May 2008).
- Vinal SC (1919) The respiratory system of the Carolina locust (*Dissosteira carolina* Linne). *Journal of the New York Entomological Society* 27: 19–32.
- Weis-Fogh T (1952) Fat combustion and metabolic rate of flying insects (*Schistocera gregaria* Forskål). *Philosophical Transactions B* 237: 1–36.
- Weis-Fogh T (1956a) The ventilatory mechanism during flight of insects in relation to the call for oxygen. *Proceedings of the XIV International Congress of Zoology* 14: 283–285.
- Weis-Fogh T (1956b) Biology and physics of locust flight. II. Flight performance of the desert locust (*Schistocera gregaria*). *Philosophical Transactions B* 239: 459–510.
- Weis-Fogh T (1956c) Biology and physics of locust flight. IV. Notes on sensory mechanisms in locust flight. *Philosophical Transactions B* 239: 555–584.
- Weis-Fogh T (1964a) Functional design of the tracheal system of flying insects as compared with the avian lung. *Journal of Experimental Biology* 41: 207–227.
- Weis-Fogh T (1964b) Diffusion in insect wing muscle, the most active tissue known. *Journal of Experimental Biology* 41: 229–256.
- Weis-Fogh T (1964c) Biology and physics of locust flight. VIII. Lift and metabolic rate of flying locusts. *Journal of Experimental Biology* 41: 257–271.
- Weis-Fogh T (1967) Respiration and tracheal ventilation in locusts and other flying insects. *Journal of Experimental Biology* 47: 561–587.
- Wigglesworth VB (1950) A new method of injecting the trachea and tracheoles of insects. *Quarterly Journal of Microscopical Science* 91: 113–137.